PHOTONICS Research

Pump scheme optimization of an incoherently pumped high-power random fiber laser

Jun Ye,[1] Jiangming Xu,[1,*] Jiaxin Song,[1] Yang Zhang,[1] Hanwei Zhang,[1] Hu Xiao,[1] Jinyong Leng,[1] and Pu Zhou[1,2]

[1]College of Advanced Interdisciplinary Studies, National University of Defense Technology, Changsha 410073, China
[2]e-mail: zhoupu203@163.com
*Corresponding author: jmxu1988@163.com

Received 30 April 2019; revised 14 June 2019; accepted 4 July 2019; posted 5 July 2019 (Doc. ID 366347); published 7 August 2019

Optical signal-to-noise ratio (OSNR) is one of the most significant parameters for the performance characterization of random fiber lasers (RFLs) and their application potentiality in sensing and telecommunication. An effective way to improve the OSNR of RFLs is pump scheme optimization, for example, employing a temporally stable source as the pump. In this paper, the output performance of an incoherently pumped RFL dependence on the pump bandwidth has been investigated both in experiment and theory. It is found that a high-OSNR RFL can be achieved with broadband amplified spontaneous emission (ASE) source pumping, and a relatively broad pump bandwidth can also help suppress the spectral broadening while maintaining an ultra-high spectral purity. By optimizing the pump bandwidth to ~10 nm, maximum OSNR of ~39 dB (corresponding to a spectral purity of ~99.96%) with more than 99 W output power can be obtained. Moreover, for the pump bandwidth of 0.6–40 nm, the spectral purity can reach as high as >99% with the pump power ranging from ~85 to ~117 W. In addition, with the aid of theoretical simulation based on a modified power balance model, we find that the increment of pump bandwidth can decrease the effective Raman gain coefficient, further influencing the gain characteristics, nonlinear effects, and eventually the output performance. This work provides new insight into the influence of the pump characteristics on the output performance of incoherently pumped RFLs.

https://doi.org/10.1364/PRJ.7.000977

1. INTRODUCTION

Random fiber lasers (RFLs), which operate via Raman gain and random distributed feedback (RDFB), have attracted increasing attention since their first demonstration in 2010 [1]. Compared with the traditional fiber lasers, RFLs employ random Rayleigh scattering (RS) along the passive fiber instead of a precise cavity to provide the feedback, making the system much simpler in structure and more economic in cost [2]. After nearly a decade of effort, a great deal of progress concerning RFLs has been made in aspects such as power scaling [3–5], linewidth narrowing [6–8], wavelength tuning and expansion [9–11], and pulsed operation [12–14]. Meanwhile, RFLs have also shown enormous application potentiality in the fields of sensing and telecommunication [15–17], frequency conversion in second-harmonic generation [18,19], power amplification [20–22], and so on [23–26].

However, most of the previously reported RFLs employ coherent fiber lasers as the pump source, which usually leads to temporal instability of the output emission due to the self-pulsing characteristic of the pump source. By adding a long section of passive fiber to stabilize the pump source, Zhang *et al.* reported a ninth-order cascaded RFL with excellent temporal stability; nevertheless, the optical signal-to-noise ratio (OSNR) of the first-order Stokes wave is still limited to <30 dB [27]. By contrast, when pumped by an incoherent amplified spontaneous emission (ASE) source, temporally stable high-power random lasing can also be obtained [28,29]. In 2017, Xu *et al.* demonstrated a powerful linearly polarized second-order RFL with a broadband ASE pumping, in which more than 100 W output power at 1178 nm was successfully achieved [29]. However, even at the maximum pump power, there still exist some unconverted pump waves which eventually result in an imperfect OSNR of ~21 dB. It is believed that the Raman gain can be less for broadband pumping, and thus the broad linewidth (3 dB linewidth of ~9.1 nm) of the ASE source should be responsible for the incomplete pump conversion. In 2018, with a narrowband filtered (<1 nm) ASE source pumping, Dong *et al.* reported a 6.9 W, eighth-order cascaded RFL at 1691.6 nm, in which the spectral purity was over 97.7% from the first- to the third-order Stokes wave, and for all eight Stokes orders, the spectral purities reached more than 90% [30]. Recently, by utilizing a novel filtered feedback mechanism

and a narrowband-filtered (3 dB linewidth of ~2.5 nm) ASE source as the pump, Balaswamy *et al.* developed a cascaded RFL with near-complete conversion over wide wavelength and power tuning, where wavelength conversions >97% were achieved over a broad (1.1–1.5 μm) tuning range, and the best spectral purity of the first-order Stokes wave reaches as high as ~99.6% [31]. These two results confirm that temporal stability of the pump source is significant for improving the OSNR (or spectral purity) of RFLs. However, it is believed that narrowband ASE pumping is necessary to achieve complete pump conversion (high spectral purity). But in fact, the Raman gain extends over a large frequency range, with a broad peak near 13 THz [32], and on an intuitive level, near-complete pump conversion can also be realized with broadband pumping. Therefore, the spectral and power characteristics of an ASE-pumped RFL dependence on pump bandwidth, which have not been discussed in previous reports, awaken our interest and curiosity.

In this paper, by utilizing a bandwidth-adjustable ASE source as the pump, we have experimentally and theoretically investigated the spectral and power characteristics of an RFL as functions of the pump bandwidth. It is found that high-OSNR RFLs can be achieved with broadband ASE pumping, and a relatively broad pump bandwidth can also help suppress the spectral broadening while maintaining an ultra-high spectral purity. As a result, by optimizing the pump bandwidth to ~10 nm, a maximum OSNR of ~39 dB (corresponding to a spectral purity of ~99.96%) with >99 W output power can be obtained. Additionally, for the pump bandwidth of 0.6–40 nm, the spectral purity can reach as high as >99%, with the pump power ranging from ~85 to ~117 W. Furthermore, a modified power balance model which takes into account the pump spectrum and frequency-dependent Raman gain can well explain the experimental results. We also found that the increment of pump bandwidth can decrease the effective Raman gain coefficient, further affecting the gain characteristics, nonlinear effects, and eventually the output performance. This work provides new insight into the influence of the pump characteristics on the output performance of incoherently pumped RFLs.

2. EXPERIMENTAL SETUP

The experimental setup of the RFL is schematically shown in Fig. 1. A homemade high-power ASE source with linewidth tunability is utilized as the pump source, which is based on the master oscillator power amplifier (MOPA) configuration, and consists of a broadband ASE seed, bandwidth-adjustable optical filter, two stages of pre-amplifiers, and a main amplifier [33,34]. The maximal operating power of the bandwidth-adjustable

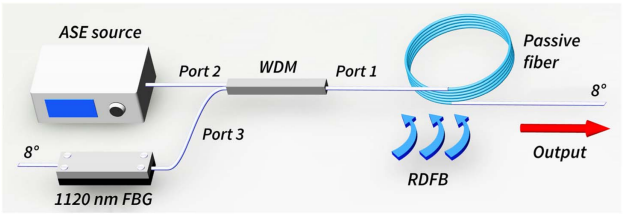

Fig. 1. Experimental setup of the incoherently pumped RFL. ASE, amplified spontaneous emission; FBG, fiber Bragg grating; WDM, wavelength division multiplexer; RDFB, random distributed feedback.

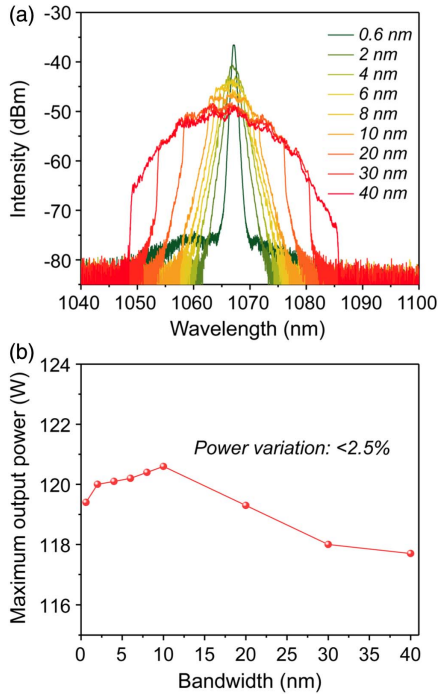

Fig. 2. (a) Bandwidth-tunable spectra of the ASE source at the maximum power level (measured after the WDM). (b) Maximum output power of the ASE source dependence on the bandwidth.

ASE source can reach as high as ~120 W. The pump wave is injected through the 1070 nm port (port 2) of a wavelength division multiplexer (WDM) with an insertion loss of 0.28 dB. The common port (port 1) of the WDM is spliced with a spool of 375 m long passive fiber to provide the RDFB, and the passive fiber features a 10 μm diameter core and 125 μm diameter clad size with a core NA of 0.08. A fiber Bragg grating with a high reflectivity of 99.7% and full width at half maximum bandwidth of 1.65 nm at the center wavelength of 1120.04 nm is spliced with the 1120 nm port (port 3) of the WDM to produce point feedback, thus constructing a half-opened cavity. In addition, all the end facets are cleaved at an angle of 8° to suppress the unwanted backward reflection.

Figure 2(a) displays the bandwidth-tunable spectra of the ASE source at the maximum power level (measured after the WDM). Here we must point out that, for the sake of convenience in description, we use "pump bandwidth" to represent the spectral coverage of the pump source. In fact, it means the passband of the filter inside the ASE source. With tuning the bandwidth from 0.6 to 40 nm, the spectral power density declines significantly. Nevertheless, the maximum output power with any bandwidth exhibits an excellent consistency. As shown in Fig. 2(b), the maximum output power of the ASE source rarely changes with the bandwidth, indicating an average value of ~119.5 W and a fluctuation <2.5%.

3. RESULTS AND DISCUSSION

A. High OSNR RFL with Broadband ASE Pumping

First, the output performance of the RFL with a broad pump bandwidth was investigated. We adjust the passband of the

filter inside the pump source to maximal 40 nm, and analyze the spectral and power performance of the RFL. Note that with 40 nm broad filtering, the 3 dB bandwidth of the pump source is ~15 nm, which is much narrower than the filtering passband. Figure 3(a) presents the output spectrum of the RFL dependence on the pump power. When the pump power increases to 40.2 W, the 1120 nm first-order Stokes wave begins to oscillate. But until the pump power exceeds 61.5 W, lots of random spikes can be seen in the output spectra, which could be attributed to the cascaded stimulated Brillouin scattering (SBS) effect [1,29]. Also due to the RS-SBS induced power instability and high peak power, the second-order Stokes wave can be observed in the output spectrum near the threshold. As the pump power increases well above the lasing threshold, the spectrum gradually broadens and becomes much smoother. Meanwhile, the power-instability-induced second-order Stokes wave degrades rapidly. In addition, the evolution of the residual pump also shows an interesting process. Initially, the center section of the pump wave is quickly depleted due to relatively high Raman gain, and a hollow which looks similar to the upside-down Raman gain spectrum can be observed within the residual pump. With further increment of the pump power, more wavelengths of the pump wave are converted to the random lasing effectively, leading to the reduction of the whole pump wave. However, due to the divergence of the frequency-dependent Raman gain, under the measurement OSNR of ~40 dB, there still exists some unconverted pump wave near 1055 and 1080 nm (corresponding to frequency shifts from the first-order Stokes wave by ~16.4 and ~9.8 THz) whose intensities are ~36.4 and ~39.9 dB, respectively, lower than that of the first-order Stokes wave with the maximum pump power.

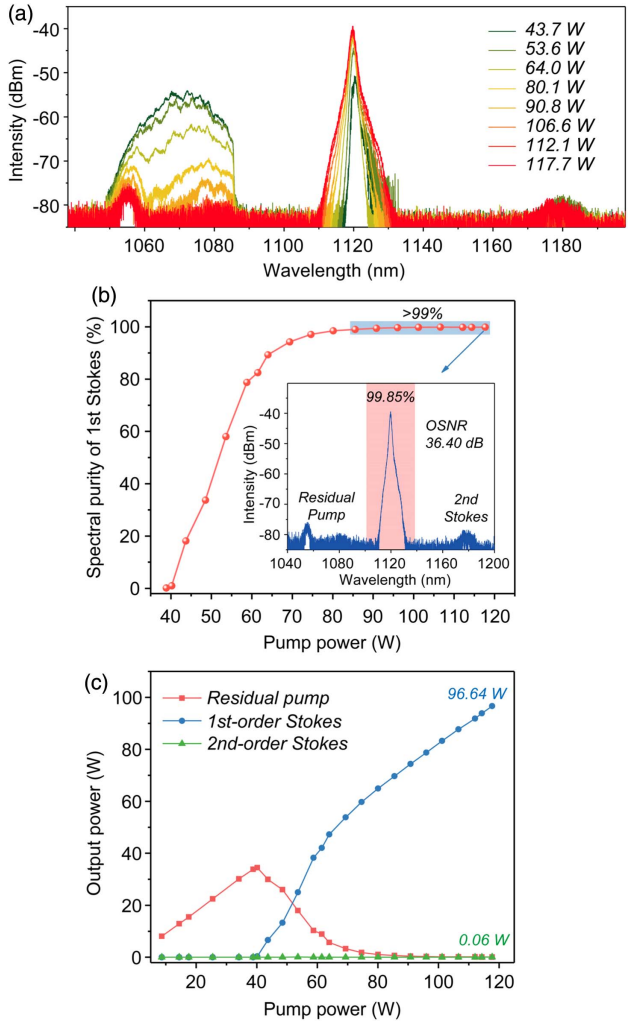

Fig. 3. (a) Evolution of the output spectrum with pump bandwidth of 40 nm. (b) Spectral purity of the first-order Stokes wave dependence on the pump power (inset: output spectrum with maximum OSNR). (c) Output powers as functions of the pump power.

Despite the weak unconverted pump wave and the second-order Stokes wave, the output spectrum also shows ultra-high OSNR and spectral purity (also known as the in-band power ratio). Figure 3(b) displays the spectral purity of the first-order Stokes wave as a function of the pump power. Before the pump power exceeds 61.5 W, the spectral purity keeps near-linear increasing with the pump power; after that, the growth rate slows down and gradually saturates. When the pump power increases to ~85.4 W, the spectral purity reaches 99%, and with the pump power ranging from 101.2 to 117.7 W, spectral purities greater than 99.8% can be achieved. As shown in the inset picture of Fig. 3(b), the maximum OSNR reaches ~36.4 dB with 117.7 W pump power, corresponding to an ultra-high spectral purity of 99.85%. We also analyzed the evolutions of the output powers, as plotted in Fig. 3(c). The pump threshold of the first-order Stokes wave is ~40.2 W, and with 117.7 W pump power, the maximum output power of 96.6 W can be obtained, corresponding to an optical-to-optical efficiency of ~82.1%. So far, thanks to the good temporal stability of the pump source, near-complete pump conversion and an ultra-high spectral purity have been achieved with broadband ASE pumping.

B. Influence of Pump Bandwidth on the Output Performance

While employing a broadband-filtered ASE source as the pump, the available bandwidth of Raman gain spectrum has an impact on the pump conversion (the existence of some unconverted pump wave near 1055 and 1080 nm). Thus, there seems to be a more optimal pump bandwidth. Figure 4(a) shows the spectra possessing maximum spectral purity with different pump bandwidth. It is seen that all the maximum OSNRs and spectral purities have exceeded 36.8 dB and 99.85%, respectively. Under the measurement OSNR of ~40 dB, the residual pump and the second-order Stokes wave can barely be observed. With the increase of pump bandwidth, there does exist some undepleted pump wave in the output spectrum; however it is so weak as to have little influence on the OSNR and spectral purity. With 10 nm pump bandwidth (3 dB bandwidth is about ~7.5 nm at the maximum operating power), an ultra-high OSNR of ~38.86 dB and spectral purity of ~99.96% can be obtained.

Figure 4(b) presents the evolutions of the spectral purity with different pump bandwidth. In a small power range above the threshold, the spectral purity keeps increasing nearly linear with the pump power, but the growth rate decreases with the increment of pump bandwidth. With the pump power ranging

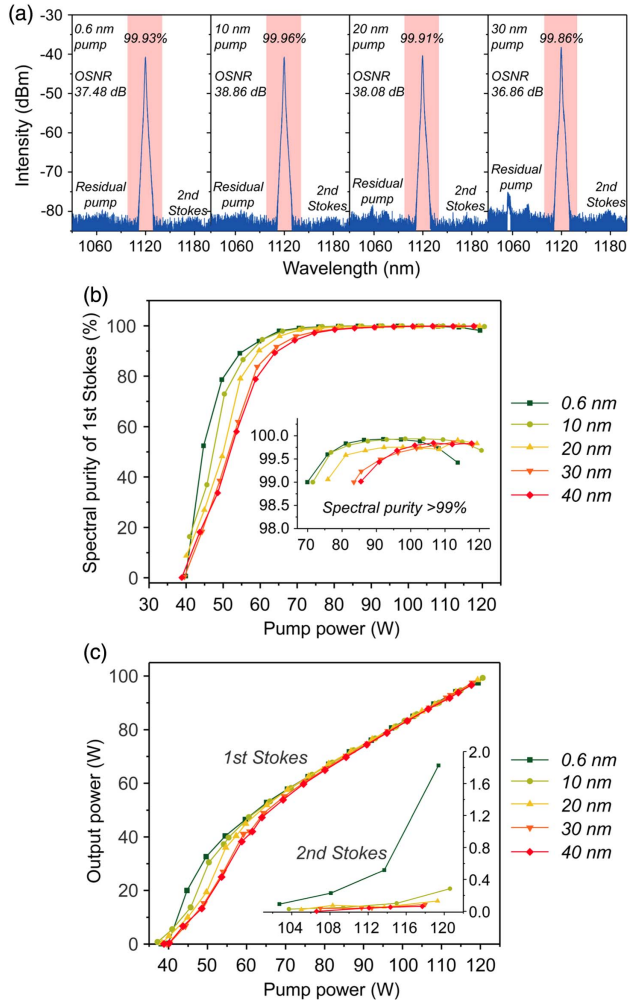

Fig. 4. (a) Spectra with maximum spectral purity at different pump bandwidth. (b) Evolutions of the spectral purity (inset: pump power range with spectral purity >99%). (c) Output powers of the first- and second-order Stokes waves (inset picture) dependence on the pump power.

from 85.4 to 115.6 W, the spectral purity with any pump bandwidth reaches more than 99%, as presented in the inset picture of Fig. 4(b). The case with 10 nm pump bandwidth covers the widest pump power range of ~49.8 W with spectral purity >99%. For all the pump bandwidths, near-complete conversion (~100% spectral purity) can be obtained with >100 W pump power. Figure 4(c) depicts the output powers of the first-order Stokes wave dependence on the pump power. The power-scaling process can be divided into two stages. In the early stage, the power-scaling curve varies with the pump bandwidth. The case with narrower pump bandwidth has a higher slope efficiency, as well as a higher absolute efficiency. With the same pump power, the narrowband pumped RFL emits more power of random lasing. The situation has been changed in the later stage, where the output power, slope efficiency, and absolute efficiency with any pump bandwidth tend to be the same. The reason could be that under the condition of near-complete pump conversion, the output powers and optical efficiencies are mainly defined by the linear

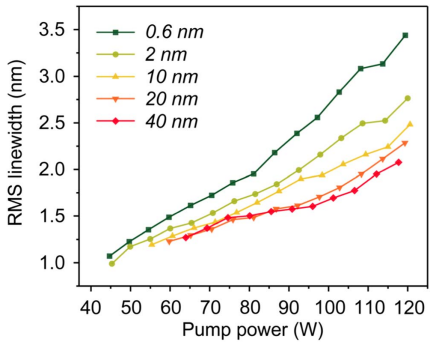

Fig. 5. Spectral broadening with different pump bandwidth.

loss of the first-order Stokes wave, and the linear loss is determined by the fiber parameters and has nothing to do with the pump bandwidth.

Furthermore, the pump bandwidth has a significant effect on the spectral broadening. Here, we use the root-mean-square (RMS) linewidth, which is an accurate and reliable parameter for describing the spectral width [32,35], to express the spectral broadening process with different pump bandwidths. It is well-known that the spectral broadening is attributed to the nonlinear effects such as self-phase modulation and cross-phase modulation [36,37]. Figure 5 shows the RMS linewidth dependence on the pump power with different pump bandwidths. It is found that the spectral broadening can be suppressed to some extent with broad pump bandwidth. For example, with 0.6 nm pump bandwidth, the RMS linewidth broadens from ~1.07 to ~3.44 nm with the pump power increasing from 44.7 to 119.4 W, while with 40 nm pump bandwidth and maximum pump power of 117.7 W, the RMS linewidth only broadens to ~2.08 nm.

C. Theoretical Investigation

To better understand the output performance of the developed RFL dependence on the pump bandwidth, we have modified the well-known power balance model in the following way. For the pump wave, spectral power densities $I_\nu = \mathrm{d}P_p/\mathrm{d}\nu$ are used to replace the total powers P_p, and the spectral dependent property of Raman gain coefficient $g_R \to g(\nu)$ is also considered. We assume that the broadband pump wave consists of numerous different frequency components, and each component can generate the Stokes wave independently with the different Raman gain coefficient $g(\nu)$. Then the modified power balance model reads [3,16,38]

$$\pm\frac{\mathrm{d}I_\nu^{\pm}}{\mathrm{d}z} = -\frac{\nu_p}{\nu_1}g(\nu)I_\nu^{\pm}(P_1^{+}+P_1^{-}+4h\nu_1\Delta\nu_1 B_1)+\varepsilon_p I_\nu^{\mp}-\alpha_p I_\nu^{\pm}, \tag{1}$$

$$\pm\frac{\mathrm{d}P_1^{\pm}}{\mathrm{d}z} = (P_1^{\pm}+2h\nu_1\Delta\nu_1 B_1)\int g(\nu)(I_\nu^{+}+I_\nu^{-})\mathrm{d}\nu - \frac{\nu_1}{\nu_2}g_{R2}(P_2^{+}+P_2^{-}+4h\nu_2\Delta\nu_2 B_2)P_1^{\pm}+\varepsilon_1 P_1^{\mp}-\alpha_1 P_1^{\pm}, \tag{2}$$

$$\pm\frac{dP_2^{\pm}}{dz}=g_{R2}(P_1^{+}+P_1^{-})(P_2^{\pm}+2h\nu_2\Delta\nu_2B_2)+\varepsilon_2P_2^{\mp}-\alpha_2P_2^{\pm}, \tag{3}$$

$$B_j=1+\frac{1}{\exp\left[\frac{h(\nu_{j-1}-\nu_j)}{k_BT}\right]-1}\qquad(j=1,2). \tag{4}$$

Here, h is the Planck constant, k_B is the Boltzmann constant, and T represents the fiber temperature. B denotes the population of the photons which introduce the noise from spontaneous Raman scattering. ν is the wave frequency and $\Delta\nu$ is the bandwidth of the Stokes wave. α, g_R, and ε denote the attenuation coefficient, Raman gain coefficient, and Rayleigh backscattering coefficient, respectively. The powers of the first- and second-order Stokes waves are represented by P_1 and P_2, correspondingly, and the boundary conditions can be described as follows:

$$P_p(0)=\int I_\nu d\nu=P_{\text{in}}, \tag{5}$$

$$P_{1,2}^{+}(0)=R_{L1,2}P_{1,2}^{-}(0), \tag{6}$$

$$P_{1,2}^{-}(L)=R_{R1,2}P_{1,2}^{+}(L), \tag{7}$$

where P_{in} is the total input pump power, and $R_{L1,2}$ and $R_{R1,2}$ denote the reflectivity of the left and right ends, respectively. The values of the parameters used for numerical calculation are listed in Table 1. In addition, the Raman gain profile is derived using the multiple-vibrational-mode model [39], and its peak value (at the frequency shift of ~13.2 THz) is set as ~0.365 $\text{km}^{-1}\cdot\text{W}^{-1}$ in the calculation.

Using this model, the evolution of the residual pump can be simulated. Figure 6(a) shows the calculated residual pump with 40 nm pump bandwidth dependence on the pump power. It is worth noting that, to simulate the measurement noise floor of the optical spectrum analyzer, we have added Gaussian white noise to the calculated residual pump. The simulated spectral evolution is in good agreement with the experimental results, in which the two-valley hollow near 1062 and 1067 nm, and the unconverted parts near 1055 and 1080 nm can be well modeled. Figures 6(b) and 6(c) depict the simulated evolution of the spectral purity and output power of the first-order Stokes wave, respectively, which are also in good agreement with the experimental evolutions. The maximum output power of the first-order Stokes wave is limited by the generation of the second-order Stokes wave. Interestingly, the pump bandwidth may have an impact on the generation of the second-order Stokes wave, and the broader the pump bandwidth, the higher the generation threshold. Thus, the output power of the first-order Stokes wave can be improved to some extent with relatively broad pump bandwidth.

Table 1. Parameters for the Numerical Calculation

Parameter	Symbol	Value
Loss	$\alpha_p,\alpha_1,\alpha_2$	$3.83, 3.70, 3.55\times10^{-4}$ m^{-1}
Bandwidth	$\Delta\nu_1,\Delta\nu_2$	0.25 THz
Wavelength	$\lambda_p,\lambda_1,\lambda_2$	1067, 1120, 1178 nm
Fiber length	L	375 m
Temperature	T	298 K
Left reflectivity	R_{L1},R_{L2}	$0.99, 4\times10^{-5}$
Right reflectivity	R_{R1},R_{R2}	4×10^{-5}
Raman gain coefficient	g_{R2}	0.365 $\text{km}^{-1}\cdot\text{W}^{-1}$
Rayleigh backscattering coefficient	$\varepsilon_0,\varepsilon_1,\varepsilon_2$	$0.34, 0.31, 0.25\times10^{-6}$ m^{-1}

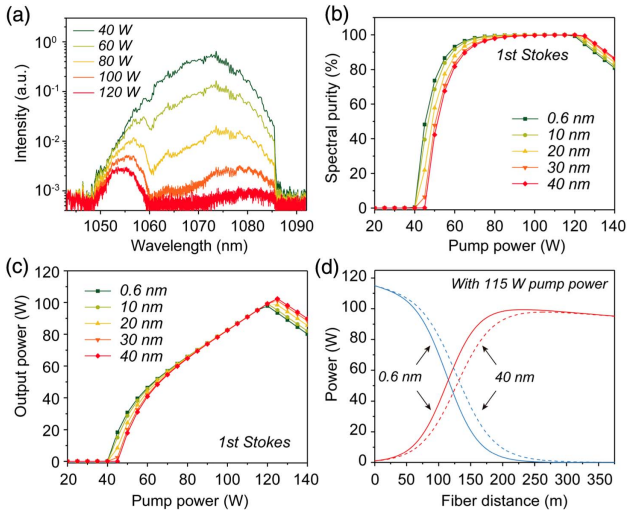

Fig. 6. (a) Calculated residual pump with 40 nm pump bandwidth. (b) Theoretical evolutions of the spectral purity. (c) Simulated output powers of the first-order Stokes wave dependence on the pump power. (d) Longitudinal power distributions with 115 W pump power (blue line indicates the pump wave, while red line indicates the forward first Stokes wave).

The reason for this can be found in the longitudinal power distributions. As presented in Fig. 6(d), with the same pump power of 115 W, the pump bandwidth has an obvious impact on the longitudinal power distribution. With 0.6 and 40 nm pump bandwidth, the power distributions at the right end are almost the same (which result in the same output powers of first-order Stokes wave). Nevertheless, the forward first-order Stokes wave with 0.6 nm pump bandwidth reaches the maximum value at a shorter fiber distance than the case with 40 nm pump bandwidth. More precisely, the forward first-order Stokes wave with 0.6 nm pump bandwidth and 115 W pump power reaches the maximum at ~231.8 m, while that with 40 nm pump bandwidth reaches the maximum at ~264.8 m. That is, the first-order Stokes wave with 0.6 nm pump bandwidth experiences a shorter amplification length. In this case, the second-order Stokes wave can experience a longer amplification length, and thus the generation threshold of the second-order Stokes wave with 0.6 nm pump bandwidth is lower than that with 40 nm pump bandwidth. The different power distributions may also contribute to the divergence of spectral broadening, as the faster the first-order Stokes increases along the fiber distance, the stronger the nonlinear effects that will be accumulated. Therefore, compared with the case of narrowband pumping, the spectral broadening can be suppressed to some extent with broad pump bandwidth due to its relatively narrower and weaker power distribution.

So far we have noticed that, on the one hand, the broader pump bandwidth can result in more residual pump light due to the limited "effective" gain bandwidth, while on the other hand it improves the generation threshold of the second-order Stokes wave to some extent. It seems that there exists a "balance" issue for the pump bandwidth, that is, there exists an optimal pump bandwidth. However, it is difficult to predict the exact value of the optimal pump bandwidth for a general experiment setup, since both central wavelength and spectral profile of the pump wave affect the results. Despite that, we also believe that there exists a general guideline for the choice of pump bandwidth, that is, the pump bandwidth should be as broad as possible on the premise that nearly complete pump conversion can be achieved. This rule is intrinsically associated with the available bandwidth of Raman gain, which is typically 2.6–4.6 THz according to the reports on the tunable random Raman fiber lasers (corresponding to a bandwidth of 10–18 nm at 1.06 μm wavelength band) [9,40,41].

In order to further explain the influence of the pump bandwidth on the output performance, we introduce the concept of effective Raman gain coefficient $g_{R\text{-eff}}$ for the conditions of broadband pumping, which is defined as the first moment of the Raman gain spectrum:

$$g_{R\text{-eff}} = \frac{\int g(\nu) I_\nu \mathrm{d}\nu}{\int I_\nu \mathrm{d}\nu}. \tag{8}$$

It is necessary to point out here that I_ν represents the spectral power density of the injected pump wave (measured after the WDM). As long as the Raman gain profile and the central wavelength of the first-order Stokes wave are fixed, the effective Raman gain coefficient is determined by the spectral power density I_ν. Specifically, the bandwidth, central wavelength, and spectral profile (such as rectangular, Lorentz, and Gaussian shape) of the pump wave affect the effective Raman gain coefficient. Figure 7(a) shows the calculated effective Raman gain coefficient as a function of the pump bandwidth. Since the Raman gain spectrum possesses a broad peak (~10 nm) [2,32], the effective Raman gain coefficient slightly decreases with pump bandwidth less than 10 nm, and thus the calculated spectral and power evolutions with the pump bandwidth <10 nm tend to be the same [as displayed in Figs. 6(b) and 6(c)]. With increment of the pump bandwidth, the effective Raman gain coefficient further decreases, which is reduced by ~11.3% compared with that of the minimal pump bandwidth.

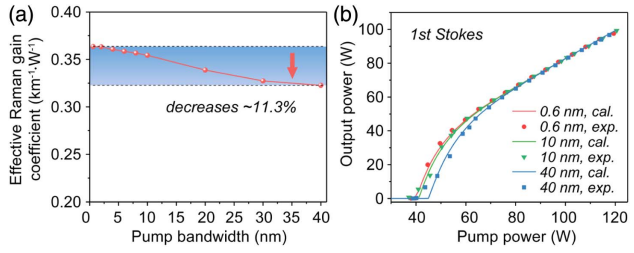

Fig. 7. (a) Effective Raman gain coefficient as a function of the pump bandwidth. (b) Evolutions of the output power with 0.6, 10, and 40 nm pump bandwidth (cal., calculated results based on the unmodified power balance model with the effective Raman gain coefficient; exp., experimental data).

The decrease of the effective Raman gain coefficient is responsible for the higher generation threshold and longer amplification length of the first-order Stokes wave.

Using the effective Raman gain coefficient, the power characteristics of the RFL can be simulated by directly using the unmodified power balance model (which consumes far less time and computer memory). As a simple verification, Fig. 7(b) displays the power scaling process with 0.6, 10, and 40 nm pump bandwidth. It is seen that the simulation results employing the unmodified power balance model with the effective Raman gain coefficient match well with the experimental data. The mismatch near the generation threshold with broad pump bandwidth can be attributed to the RS-SBS induced temporal instability, which leads to the earlier generation of the first-order Stokes wave than the calculation. Another possible reason may be the "hole burning" effect, which is caused by the divergence of the Raman gain coefficient of different pump components. The central pump components can exhibit lower lasing thresholds than the side-band pump components, while the effective Raman gain coefficient is an average value, so that it fails to include the particularity of the central pump components, thus resulting in the discrepancy between the modeling and experiment near the threshold.

4. CONCLUSION

In summary, with bandwidth-adjustable ASE pumping, we investigated the spectral and power characteristics of the RFL dependence on the pump bandwidth. The experimental results show that high-OSNR RFL can also be achieved with broadband ASE pumping, and a relatively broad pump bandwidth can help boost the maximum output power to some extent, as well as suppress the spectral broadening while maintaining an ultra-high spectral purity. As a result, by optimizing the pump bandwidth to ~10 nm, a maximum OSNR of ~39 dB (corresponding to a spectral purity of ~99.96%) with over 99 W output power can be obtained. Furthermore, for the pump bandwidth of 0.6–40 nm, the spectral purity reaches more than 99% with the pump power ranging from ~85 to ~117 W. Additionally, by considering the pump spectrum and frequency-dependent Raman gain, we demonstrate a modified power balance model by which the spectral and power characteristics can be well simulated. In addition, it is found that the increment of pump bandwidth can decrease the effective Raman gain coefficient, further influencing the gain characteristics and nonlinear effects, and eventually affecting the longitudinal power distribution and output performance such as the power scaling process, achievable maximum OSNR, and even the high-order Stokes generation threshold. This work provides a more optimized scheme for high-power, high OSNR RFLs, and may provide new insight into the influence of the pump characteristics on the output performance of incoherently pumped RFLs.

Funding. National Natural Science Foundation of China (NSFC) (61635005); Natural Science Foundation of Hunan Province (2018JJ3588); Huo Yingdong Education Foundation (151062).

REFERENCES

1. S. K. Turitsyn, S. A. Babin, A. E. El-Taher, P. Harper, D. V. Churkin, S. I. Kablukov, J. D. Ania-Castañón, V. Karalekas, and E. V. Podivilov, "Random distributed feedback fibre laser," Nat. Photonics **4**, 231–235 (2010).
2. S. K. Turitsyn, S. A. Babin, D. V. Churkin, I. D. Vatnik, M. Nikulin, and E. V. Podivilov, "Random distributed feedback fibre lasers," Phys. Rep. **542**, 133–193 (2014).
3. Z. Wang, H. Wu, M. Fan, L. Zhang, Y. Rao, W. Zhang, and X. Jia, "High power random fiber laser with short cavity length: theoretical and experimental investigations," IEEE J. Sel. Top. Quantum Electron. **21**, 0900506 (2015).
4. H. Zhang, L. Huang, P. Zhou, X. Wang, J. Xu, and X. Xu, "More than 400 W random fiber laser with excellent beam quality," Opt. Lett. **42**, 3347–3350 (2017).
5. H. Zhang, J. Ye, P. Zhou, X. Wang, J. Leng, J. Xu, J. Wu, and X. Xu, "Tapered-fiber-enabled high-power, high-spectral-purity random fiber lasing," Opt. Lett. **43**, 4152–4155 (2018).
6. S. Sugavanam, N. Tarasov, X. Shu, and D. V. Churkin, "Narrow-band generation in random distributed feedback fiber laser," Opt. Express **21**, 16466–16472 (2013).
7. M. Pang, X. Bao, and L. Chen, "Observation of narrow linewidth spikes in the coherent Brillouin random fiber laser," Opt. Lett. **38**, 1866–1868 (2013).
8. J. Ye, J. Xu, H. Zhang, and P. Zhou, "Powerful narrow linewidth random fiber laser," Photon. Sens. **7**, 82–87 (2017).
9. S. A. Babin, A. E. El-Taher, P. Harper, E. V. Podivilov, and S. K. Turitsyn, "Tunable random fiber laser," Phys. Rev. A **84**, 021805 (2011).
10. L. Zhang, H. Jiang, X. Yang, W. Pan, S. Cui, and Y. Feng, "Nearly-octave wavelength tuning of a continuous wave fiber laser," Sci. Rep. **7**, 42611 (2017).
11. X. Jin, Z. Lou, H. Zhang, J. Xu, P. Zhou, and Z. Liu, "Random distributed feedback fiber laser at 2.1 μm," Opt. Lett. **41**, 4923–4926 (2016).
12. M. Bravo, M. Fernandez-Vallejo, and M. Lopez-Amo, "Internal modulation of a random fiber laser," Opt. Lett. **38**, 1542–1544 (2013).
13. B. Yao, Y. Rao, Z. Wang, Y. Wu, J. Zhou, H. Wu, M. Fan, X. Cao, W. Zhang, Y. Chen, Y. Li, D. Churkin, S. Turitsyn, and C. Wong, "Graphene based widely-tunable and singly-polarized pulse generation with random fiber lasers," Sci. Rep. **5**, 18526 (2016).
14. W. Pan, L. Zhang, H. Jiang, X. Yang, S. Cui, and Y. Feng, "Ultrafast Raman fiber laser with random distributed feedback," Laser Photon. Rev. **12**, 1700326 (2018).
15. Z. N. Wang, Y. J. Rao, H. Wu, P. Y. Li, Y. Jiang, X. H. Jia, and W. L. Zhang, "Long-distance fiber-optic point-sensing systems based on random fiber lasers," Opt. Express **20**, 17695–17700 (2012).
16. D. V. Churkin, S. Sugavanam, I. D. Vatnik, Z. Wang, E. V. Podivilov, S. A. Babin, Y. Rao, and S. K. Turitsyn, "Recent advances in fundamentals and applications of random fiber lasers," Adv. Opt. Photon. **7**, 516–569 (2015).
17. Y. Xu, L. Zhang, S. Gao, P. Lu, S. Mihailov, and X. Bao, "Highly sensitive fiber random-grating-based random laser sensor for ultrasound detection," Opt. Lett. **42**, 1353–1356 (2017).
18. E. I. Dontsova, S. I. Kablukov, I. D. Vatnik, and S. A. Babin, "Frequency doubling of Raman fiber lasers with random distributed feedback," Opt. Lett. **41**, 1439–1442 (2016).
19. S. Rota-Rodrigo, B. Gouhier, C. Dixneuf, L. Antoni-Micollier, G. Guiraud, D. Leandro, M. Lopez-Amo, N. Traynor, and G. Santarelli, "Watt-level green random laser at 532 nm by SHG of a Yb-doped fiber laser," Opt. Lett. **43**, 4284–4287 (2018).
20. X. Du, H. Zhang, P. Ma, H. Xiao, X. Wang, P. Zhou, and Z. Liu, "Kilowatt-level fiber amplifier with spectral-broadening-free property, seeded by a random fiber laser," Opt. Lett. **40**, 5311–5314 (2015).
21. T. Li, Y. Li, W. Ke, C. Zha, W. Peng, Y. Sun, and Y. Ma, "Power scaling of narrow-linewidth fiber amplifier seeded by Yb-doped random fiber laser," IEEE J. Sel. Top. Quantum Electron. **24**, 0903208 (2018).
22. J. Xu, J. Ye, P. Zhou, J. Leng, H. Xiao, H. Zhang, J. Wu, and J. Chen, "Tandem pumping architecture enabled high power random fiber laser with near-diffraction-limited beam quality," Sci. China Technol. Sci. **62**, 80–86 (2019).
23. R. Ma, Y. J. Rao, W. L. Zhang, and B. Hu, "Multimode random fiber laser for speckle free imaging," IEEE J. Sel. Top. Quantum Electron. **25**, 0900106 (2018).
24. X. Jin, X. Du, X. Wang, P. Zhou, H. Zhang, X. Wang, and Z. Liu, "High-power ultralong-wavelength Tm-doped silica fiber laser cladding-pumped with a random distributed feedback fiber laser," Sci. Rep. **6**, 30052 (2016).
25. H. Wu, P. Wang, J. Song, J. Ye, J. Xu, X. Li, and P. Zhou, "High power tunable mid-infrared optical parametric oscillator enabled by random fiber laser," Opt. Express **26**, 6446–6455 (2018).
26. R. Ma, Y. J. Rao, W. L. Zhang, X. Zeng, X. Dong, H. Wu, Z. N. Wang, and X. P. Zeng, "Backward supercontinuum generation excited by random lasing," IEEE J. Sel. Top. Quantum Electron. **24**, 0901105 (2018).
27. L. Zhang, J. Dong, and Y. Feng, "High-power and high-order random Raman fiber lasers," IEEE J. Sel. Top. Quantum Electron. **24**, 1400106 (2018).
28. J. Xu, P. Zhou, W. Liu, J. Leng, H. Xiao, P. Ma, J. Wu, H. Zhang, J. Chen, and Z. Liu, "Exploration in performance scaling and new application avenues of superfluorescent fiber source," IEEE J. Sel. Top. Quantum Electron. **24**, 0900710 (2018).
29. J. Xu, Z. Lou, J. Ye, J. Wu, J. Leng, H. Xiao, H. Zhang, and P. Zhou, "Incoherently pumped high-power linearly-polarized single-mode random fiber laser: experimental investigations and theoretical prospects," Opt. Express **25**, 5609–5617 (2017).
30. J. Dong, L. Zhang, H. Jiang, X. Yang, W. Pan, S. Cui, X. Gu, and Y. Feng, "High order cascaded Raman random fiber laser with high spectral purity," Opt. Express **26**, 5275–5280 (2018).
31. V. Balaswamy, S. Ramachandran, and V. R. Supradeepa, "High-power, cascaded random Raman fiber laser with near complete conversion over wide wavelength and power tuning," Opt. Express **27**, 9725–9732 (2019).
32. G. P. Agrawal, *Nonlinear Fiber Optics* (Academic, 2013).
33. J. Xu, J. Ye, H. Xiao, J. Leng, W. Liu, and P. Zhou, "In-band pumping avenue based high power superfluorescent fiber source with record power and near-diffraction-limited beam quality," High Power Laser Sci. Eng. **6**, e46 (2018).
34. J. Ye, J. Xu, Y. Zhang, J. Song, J. Leng, and P. Zhou, "Spectrum-manipulable hundred-watt-level high power superfluorescent fiber source," J. Lightwave Technol. **37**, 3113–3118 (2019).
35. W. Liu, P. Ma, P. Zhou, and Z. Jiang, "Spectral property optimization for a narrow-band-filtered superfluorescent fiber source," Laser Phys. Lett. **15**, 025103 (2018).
36. S. A. Babin, E. A. Zlobina, S. I. Kablukov, and E. V. Podivilov, "High-order random Raman lasing in a PM fiber with ultimate efficiency and narrow bandwidth," Sci. Rep. **6**, 22625 (2016).
37. A. E. Budarnykh, I. A. Lobach, E. A. Zlobina, V. V. Velmiskin, S. I. Kablukov, S. L. Semjonov, and S. A. Babin, "Raman fiber laser with random distributed feedback based on a twin-core fiber," Opt. Lett. **43**, 567–570 (2018).
38. D. V. Churkin, S. A. Babin, A. E. El-Taher, P. Harper, S. I. Kablukov, V. Karalekas, J. D. Ania-Castañón, E. V. Podivilov, and S. K. Turitsyn, "Raman fiber lasers with a random distributed feedback based on Rayleigh scattering," Phys. Rev. A **82**, 033828 (2010).
39. D. Hollenbeck and C. D. Cantrell, "Multiple-vibrational-mode model for fiber-optic Raman gain spectrum and response function," J. Opt. Soc. Am. B **19**, 2886–2892 (2002).
40. A. R. Sarmani, R. Zamiri, M. H. A. Bakar, B. Z. Azmi, A. W. Zaidan, and M. A. Mahdi, "Tunable Raman fiber laser induced by Rayleigh back-scattering in an ultra-long cavity," J. Eur. Opt. Soc. Rapid Publ. **6**, 11043 (2011).
41. J. Song, H. Wu, J. Ye, H. Zhang, J. Xu, P. Zhou, and Z. Liu, "Investigation on extreme frequency shift in silica fiber-based high-power Raman fiber laser," High Power Laser Sci. Eng. **6**, e28 (2018).